

Article

Ultra-Broadband Angular-Stable Reflective Linear to Cross Polarization Converter

Bianmei Zhang ^{1,2}, Chenghui Zhu ¹, Ran Zhang ¹, Xiaofan Yang ³, Ye Wang ¹ and Xiaoming Liu ^{1,4,*}¹ School of Physics and Electronic Information, Anhui Normal University, Wuhu 241002, China² School of Electrical and Electronic Engineering, Anhui Institute of Information Technology, Wuhu 241002, China³ The State Key Laboratory of Complex Electromagnetic Environment Effects on Electronic and Information System, Luoyang 471004, China⁴ Wuhu CEPREI Information Industry Technology Research Institute, Wuhu 241002, China

* Correspondence: xiaoming.liu@ahnu.edu.cn

Abstract: An ultra-broadband angular-stable reflective linear to cross polarization converter based on metasurface is developed. The unit cell of the converter is formed by a slant end-loaded H-shaped resonator. The slant arrangement is to create polarization conversion. The end-loaded stubs are useful for miniaturization and the slots are responsible for enlarging bandwidth. The simulated results show that the polarization conversion ratio of the proposed design is better than 90% in the range of 9.83–29.37 GHz, corresponding to a relative bandwidth of 99.69%. It is also demonstrated that the mean polarization conversion ratio is larger than 80% even though the incident angle reaches 40° for both *x*-polarized and *y*-polarized incidences. To validate the design, a prototype of the proposed structure is fabricated and measured. Satisfactory agreement has been observed between measurement and simulation. Compared with the designs in the literature, the developed converter exhibits good performance of high efficiency, ultra-broadband and angular stability. Potential applications can be expected in polarization-controlled devices, stealth surfaces, antennas, etc.

Keywords: polarization converter; ultra-broadband; angular stability; metasurface; polarization conversion ratio



Citation: Zhang, B.; Zhu, C.; Zhang, R.; Yang, X.; Wang, Y.; Liu, X. Ultra-Broadband Angular-Stable Reflective Linear to Cross Polarization Converter. *Electronics* **2022**, *11*, 3487. <https://doi.org/10.3390/electronics11213487>

Academic Editors: Naser Ojaroudi Parchin, Mohammad Ojaroudi and Raed A. Abd-Alhameed

Received: 8 October 2022
Accepted: 25 October 2022
Published: 27 October 2022

Publisher's Note: MDPI stays neutral with regard to jurisdictional claims in published maps and institutional affiliations.



Copyright: © 2022 by the authors. Licensee MDPI, Basel, Switzerland. This article is an open access article distributed under the terms and conditions of the Creative Commons Attribution (CC BY) license (<https://creativecommons.org/licenses/by/4.0/>).

1. Introduction

The polarization of a train of electromagnetic (EM) waves refers to the oscillating direction of its electric field in the plane perpendicular to the propagation direction [1]. Effective controlling or manipulating of polarization state is frequently required in many applications [2,3]. Traditional methods for polarization control include making uses of the birefringence effect and optical activity of natural materials [4–7]. However, these methods usually lead to a bulky thickness. Over the past decade, great efforts were devoted to the investigation of planar periodical structures, also called metasurfaces (MSs) due to their fascinating functionalities that cannot be found in conventional materials, such as negative refraction [8], superlens [9], invisibility cloak [10,11], perfect absorption [12] and so on. Metasurfaces also provide an efficient approach to polarization control in sub-wavelength scale [13–15]. In particular, by utilizing this method, the thickness may be significantly reduced.

In recent years, polarization converters based on anisotropic MSs have been intensively studied. In general, MS-based polarization converters can be classified into two types, i.e., the transmission type and the reflection type. Many of them have been reported over the microwave [16–18] and terahertz [19,20] ranges. For the transmission type, broadband polarization converters are frequently realized by staking multilayer structures [21–23]. However, its complex structure makes it less convenient to be fabricated. In contrast, the

reflection type is capable of creating high-efficiency and broadband polarization conversion using monolayer MSs [24–29].

For instance, Zheng et al. [26] developed a polarization converter based on a modified H-shaped resonator that achieved linear polarization conversion with a bandwidth <61%. Li et al. [27] proposed another reflective polarization converter based on the square splitting resonators. The bandwidth was increased to 94% for polarization conversion ratio (PCR) greater than 80%. However, it is difficult for this design to maintain high conversion efficiency over a wide bandwidth. To increase the conversion efficiency, a perforated array was used [28,29], and the bandwidth could be as broad as 111%. Meanwhile, the PCR was better than 89% over the whole range. To further broaden the bandwidth and produce better PCR, Jia et al. [30] presented two cascaded dielectric-layer structure. Unfortunately, it only demonstrated a good efficiency for normal incidence.

Improvements have also been made to broaden both the bandwidth and the angular stability [31–36]. Karamirad et al. [31] introduced an oval pattern periodic array based on multiple plasmon resonances and surface magnetic field distributions. The bandwidth of this design was about 67% with an angular stability of 30°. Another design [32] using cross-shaped resonators enhanced the angular stability to 40°, but the bandwidth was not sufficiently wide. Wu et al. [36] presented a broadband design that consisted of hollow oval sheet and rectangle patch, providing a bandwidth up to 90% for the first band. However, this design was very sensitive to the incident angle, and only operated efficiently with 25° angular stability.

It is seen that, for a polarization converter, there is a dilemma between bandwidth, efficiency and angular stability. Therefore, investigating the development of easy fabrication, wide bandwidth and large angle stability cross-polarization converter is still worthy of a great deal of effort.

In this work, an ultra-broadband angular stable linear polarization-converter based on MS is developed. It is composed of a single layer slant end-loaded H-shaped resonator. The slant arrangement is to create polarization conversion. The end-loaded stubs are useful for miniaturization. Moreover, the slots are responsible for enlarging bandwidth. It will be demonstrated that the PCR efficiency of this design is better than 90%. Even when the incident angle reaches 40°, the mean PCR remains above 80%. It will also be demonstrated that a good tradeoff between bandwidth, PCR and angular stability has been obtained. The fabricated prototype confirms a good agreement between simulation and measurement.

2. Design and Simulation

The unit cell evolves from a simple slant dipole, as shown in Figure 1a. Following on, two U-shaped stubs are loaded with each end of the dipole, so that the unit cell is partly miniaturized without destroying polarization conversion, see Figure 1b. To enlarge its bandwidth, two slots are cut at the ends, forming an H-shaped resonator, as depicted in Figure 1c, cutting slots in a common way to enhance bandwidth in antenna design [37]. This technique is used in this design to enhance the bandwidth of polarization conversion. The dielectric layer is PTFE having a relative dielectric constant (ϵ_r) of 2.2 and a loss tangent ($\tan \delta$) of 0.0009. The thickness (h) of the substrate is 2.5 mm. The metallic layers are copper with thickness of 0.035 mm and electrical conductivity of $\sigma = 5.8 \times 10^7$ S/m. By using low loss substrate, it is possible to create a higher conversion efficiency. The resultant dimensions of the structure are $p = 6$ mm, $s = 6.28$ mm, $w = 0.28$ mm, $g = 2.2$ mm, $l_1 = 1.61$ mm, $l_2 = 1.62$ mm, $l_3 = 0.65$ mm. The unit cell has an overall size of $6 \times 6 \times 2.5$ mm³.

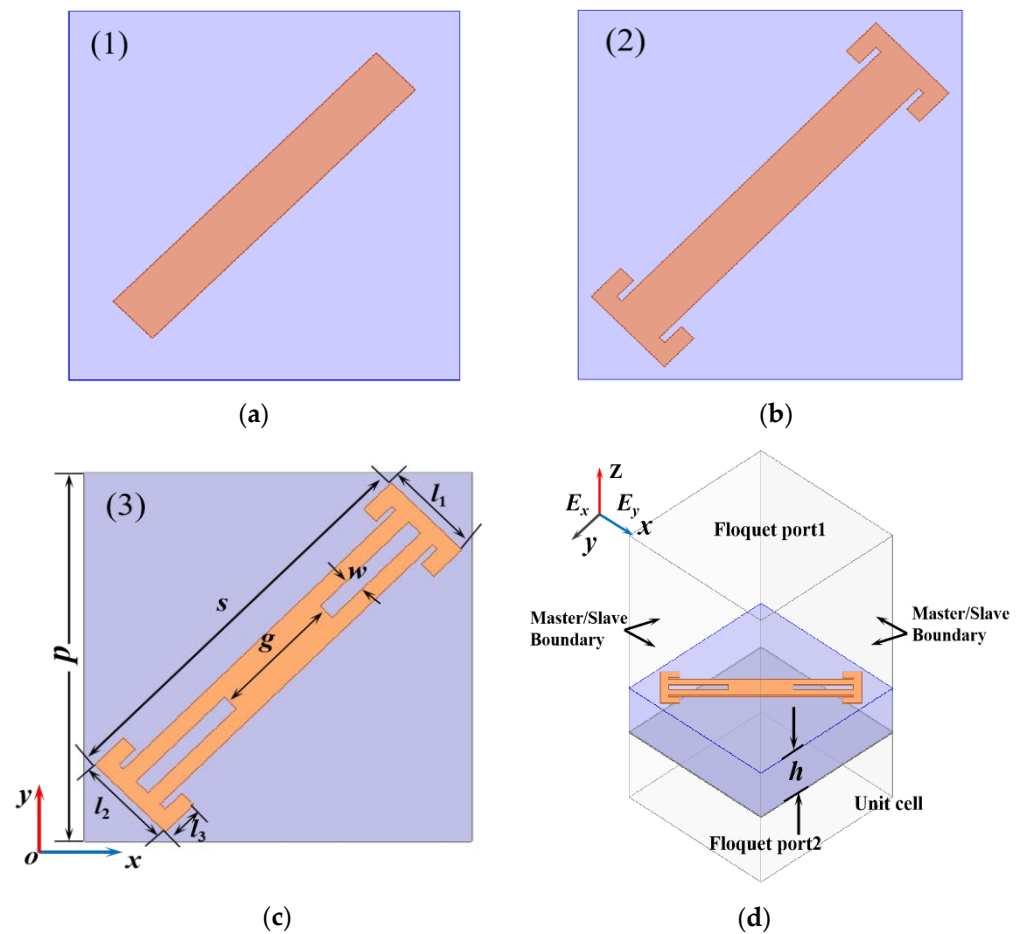


Figure 1. Evolution of the unit cell. (a) The slant dipole; (b) the end-loaded dipole; (c) the front view of the proposed polarization converter unit cell; (d) the schematic diagram of the port setting and boundary conditions for simulation.

A series of numerical simulations by using Ansoft HFSS are conducted to check the design. In the simulation model, the four boundaries are assigned as master/slave periodic conditions, as shown in Figure 1d. Since the unit cell shows mirror symmetry along its diagonal line, only the amplitudes of r_{xx} and r_{yx} along with their phase difference $\Delta\varphi_{xy} = \arg(r_{xx}) - \arg(r_{yx})$ under normal incidence for x -polarization are plotted in Figure 2. It is seen that the amplitudes of r_{xx} are smaller than -10 dB and that of r_{yx} are better than -1 dB in the range of 9.90–29.34 GHz. The phase differences $\Delta\varphi_{xy}$ are plotted in Figure 2b, where it is seen that $\Delta\varphi_{xy}$ is close to $\pm(2n + 1)90^\circ$ (n is an integer) in the whole frequency region. These simulation results indicate that x -polarization at normal incidence is converted into y -polarization within the operating band.

Another parameter used to characterize polarization conversion is the PCR of the reflected wave, which is usually defined as [26]:

$$\text{PCR} = r_{yx}^2 / (r_{yx}^2 + r_{xx}^2) = 1 - r_{xx}^2 / (r_{yx}^2 + r_{xx}^2). \tag{1}$$

The calculated PCR of the proposed design is plotted in Figure 3a. It is observed that the PCR is better than 90% in the range of 9.83–29.37 GHz, and reaches nearly 100% at the three resonance frequencies. The relative bandwidth is up to 99.69%, being broader than the designs in the literature [31–36]. Additionally, Figure 3b shows the polarization azimuth angle α to describe the angle between the major polarization axis and x -axis, which can be calculated as [25]:

$$\alpha = \arctan(r_{yx} / r_{xx}) \tag{2}$$

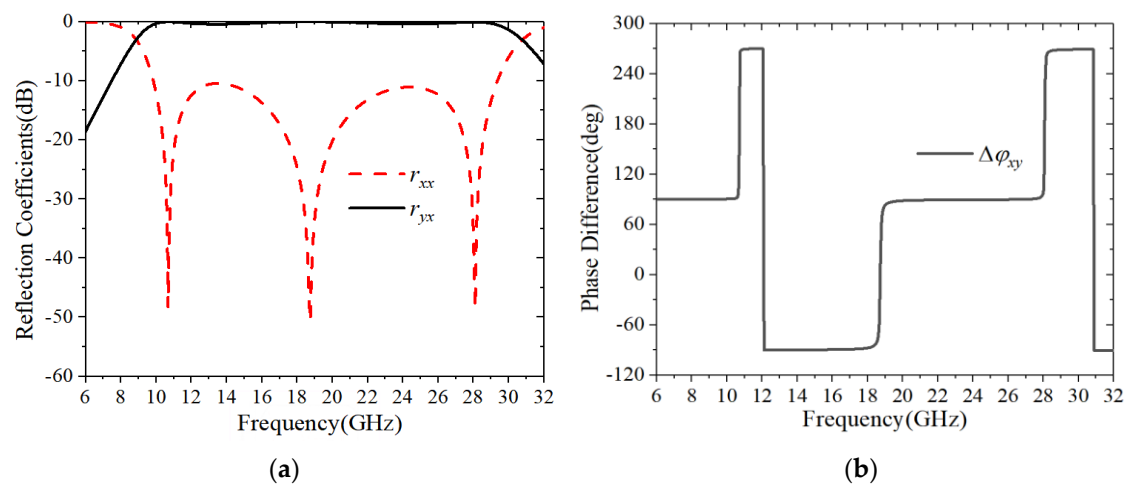


Figure 2. The simulated results of the proposed polarization converter under normal incidence for x -polarization. (a) The magnitudes of r_{xx} and r_{yx} ; (b) the phase difference $\Delta\varphi_{xy}$ between r_{xx} and r_{yx} .

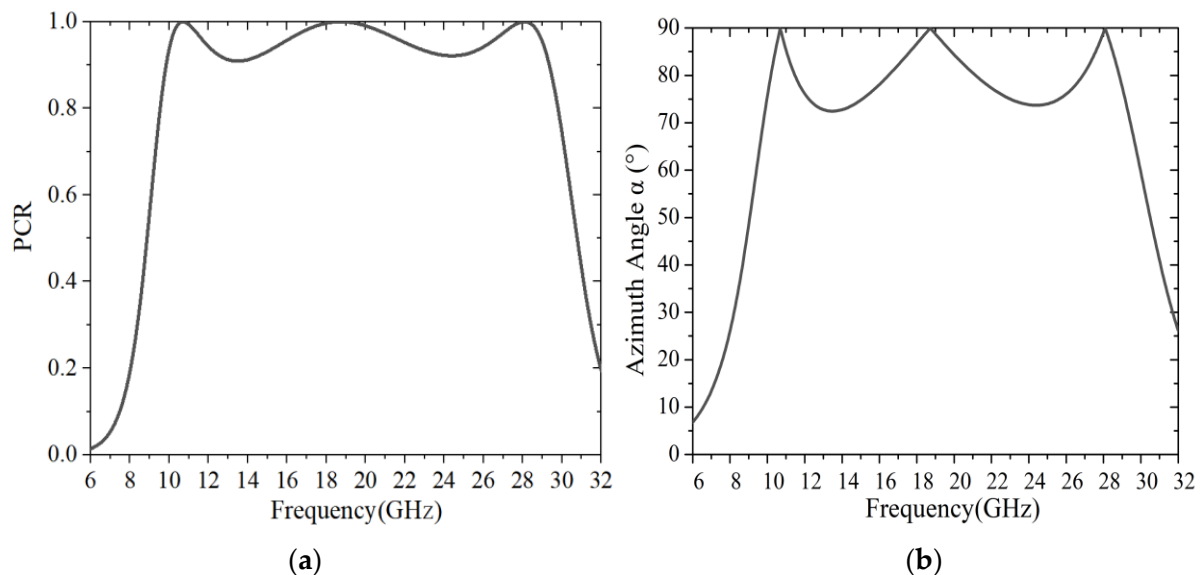


Figure 3. The simulated results for (a) PCR; (b) polarization azimuth angle α .

This is a more intuitive parameter describing frequency dependent polarization conversion. It is seen from Figure 3b that the polarization azimuth angle α is larger than 72° in the range of 9.83–29.37 GHz. The values of α approach 90° at three resonance frequencies of 10.68, 18.74 and 28.10 GHz. These results further confirm that the high-efficiency cross polarization conversion has been realized from x -polarized to y -polarized over the broad frequency bands [27].

A comparison of PCRs for each cell in Figure 1 is plotted in Figure 4. It can be found that the slant dipole array is capable of stimulating polarization rotation. However, the bandwidth of PCR does not appear to be any better compared with the other two design, though the structure is simpler. The end is then loaded two U-shaped stubs to minimize the design, which leads to an increase in resonance points. The resultant bandwidth of this structure is about 94.2% with PCR as high as 0.9. It is recognized that a wider bandwidth may be obtained by introducing slots to the structure [33]; two slots are cut in the slant dipole, as shown in Figure 1c. Such modification increases the bandwidth to 99.69%.

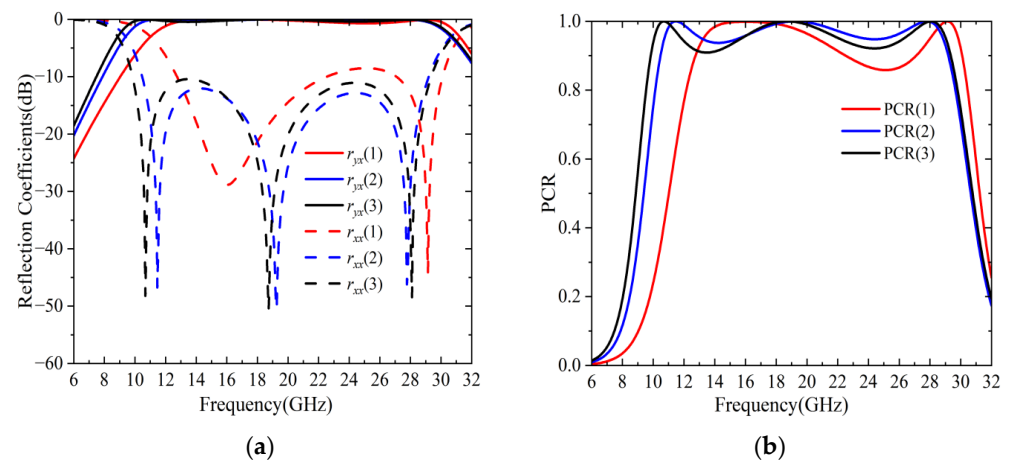


Figure 4. Simulation results for unit cells. (a) Reflective coefficients; (b) PCRs.

Another merit of the polarization converter is its angular stability. The PCR is assumed to be dependent on the incident angle. As shown in Figure 5, the PCRs for different incident angles are plotted for x -polarized and y -polarized incidences. It is apparent that the PCR bandwidth of the polarization converter gradually reduces when the incident angle increases from 0° to 40° . In the higher frequency region (around 26 GHz), the influence due to the increase in the incident angle is more pronounced, which may be attributed to the destructive interference caused by the extra path traveled by the wave inside the substrate [38]. Even though there is a decrease in the PCR bandwidth, it is seen from Figure 5a that a wide angular stability up to 20° can be observed from 10.4 to 26 GHz for the x -polarized wave. This frequency range is defined in terms of 90% PCR. For the y -polarized wave, the corresponding range is from 10.33 to 25.93 GHz. Therefore, it is seen that the polarization converter is independent from the polarization state of the incident wave. Moreover, even for 30° incidence, the PCR can be more than 85% from the range of (10.29–24.66 GHz). Furthermore, the mean PCR is still better than 80%, even though the incident angle is up to 40° . This is a piece of good evidence showing that the proposed converter has a satisfactory angular stability over the range of 0 – 40° . It should be noted that the proposed polarization converter has a cell periodicity of $0.197\lambda_{\max}$ and a thickness of $0.082\lambda_{\max}$, where λ_{\max} is the free-space wavelength corresponding to the lowest frequency in the frequency range of 9.83–29.37 GHz.

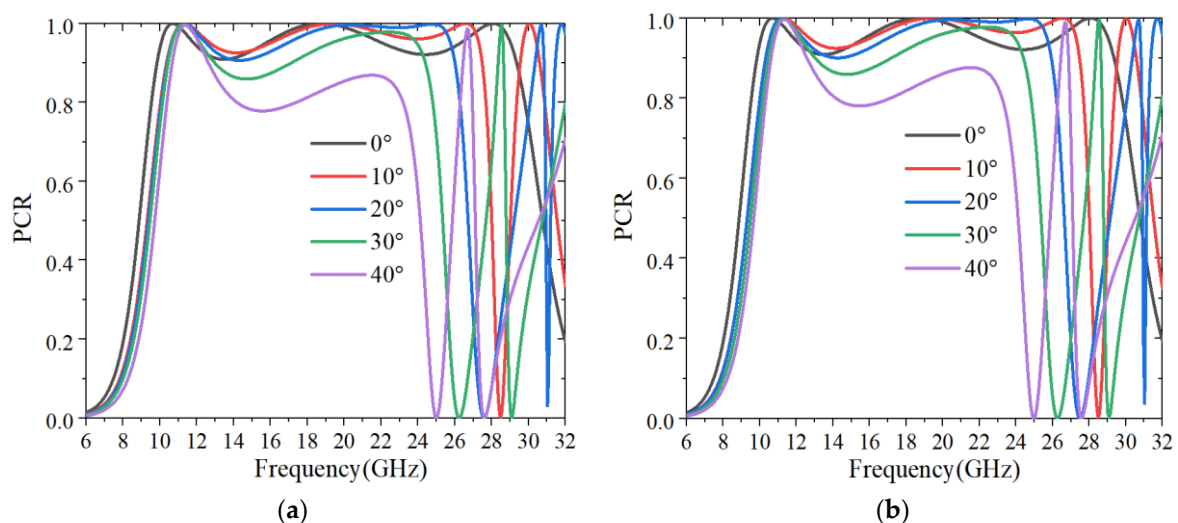


Figure 5. The PCR under different oblique incidences for (a) x -polarized wave; (b) y -polarized wave.

Actually, this design loads a U-shaped stub at each end of the dipole as resonator so as to reduce side length, which is a typical technique for miniaturization. It is recognized that the resonance characteristic of the structure is dependent on the geometric parameters of structure [31,38]. By decreasing the size of the unit cell, the resonance characteristic is better met. To study the influence of the size of the unit cell on the incident angle stability, the amplitudes of r_{xx} for different parametric sweep on incident angle vs. the size of unit cell are plotted in Figure 6. It can be seen that with the decrease in the size of unit cell, the resonant frequency of r_{xx} at lower frequencies almost remains stable, while that of r_{xx} at higher frequencies shifts towards higher frequencies, when the incident angle is kept constant. Moreover, the dip values of the resonance frequencies are better at different incident angles when the size of the unit cell gradually decreases, especially for middle resonance frequencies. It is evident that this structure will produce better PCR or wider bandwidth for the miniaturization of the unit cell, as shown in Figure 7. Therefore, the wide incident angle stability of the proposed converter can be attributed to the miniaturization of the unit cell.

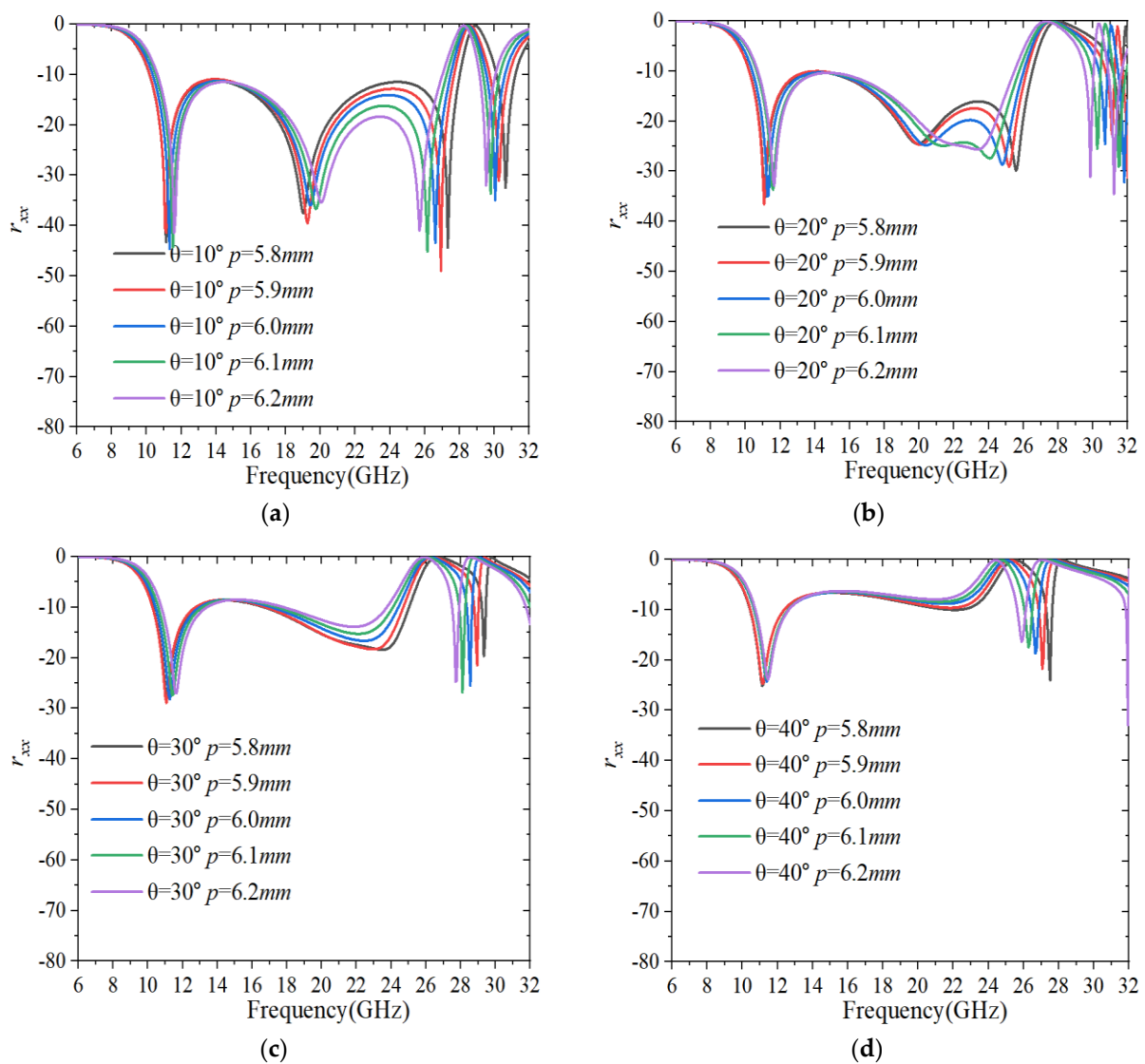


Figure 6. The amplitudes of r_{xx} for normal x -polarization incidence. (a) $\theta = 10^\circ$; (b) $\theta = 20^\circ$; (c) $\theta = 30^\circ$; (d) $\theta = 40^\circ$.

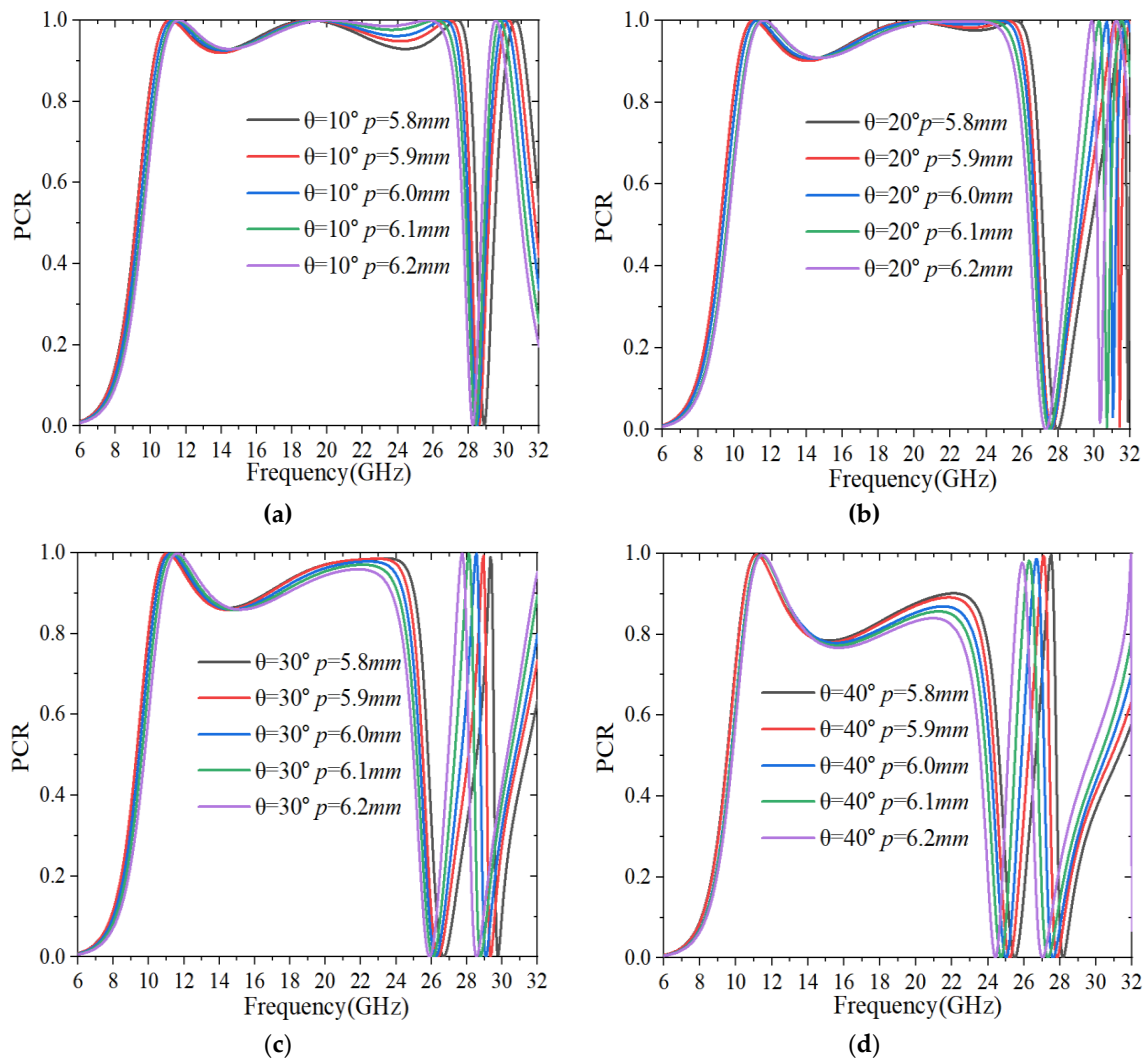


Figure 7. The PCRs for normal x-polarization incidence. (a) $\theta = 10^\circ$; (b) $\theta = 20^\circ$; (c) $\theta = 30^\circ$; (d) $\theta = 40^\circ$.

3. Analysis and Discussion

3.1. Theoretical Analysis of Linear to Cross Polarization

To understand the underlying physical mechanisms of the proposed polarization converter, a new coordinate system (the u -axis and v -axis) is usually defined to analyze the structural anisotropy. They are obtained via rotating the x -axis and y -axis counterclockwise by 45° . The x -polarized incident EM wave (\vec{E}_x^i) can be decomposed into two components along the u -axis (\vec{E}_u^i) and v -axis (\vec{E}_v^i), as shown in Figure 8a. Thus, the incident and reflected electric fields can be expressed as [26]:

$$\vec{E}_x^i = \vec{x} \left| \vec{E}_x^i \right| = \vec{x} E_0 e^{jkz} = \vec{E}_u^i + \vec{E}_v^i = \vec{u} \left| \vec{E}_u^i \right| + \vec{v} \left| \vec{E}_v^i \right|. \quad (3)$$

The reflection coefficients aligned along the u -direction and v -direction can be defined as r_{uu} and r_{vv} , respectively. Then, the reflected field can be written as [31]:

$$\vec{E}_x^r = \vec{E}_u^r + \vec{E}_v^r = \vec{u} r_{uu} \left| \vec{E}_u^i \right| e^{j(kz + \varphi_{uu})} + \vec{v} r_{vv} \left| \vec{E}_v^i \right| e^{j(kz + \varphi_{vv})}. \quad (4)$$

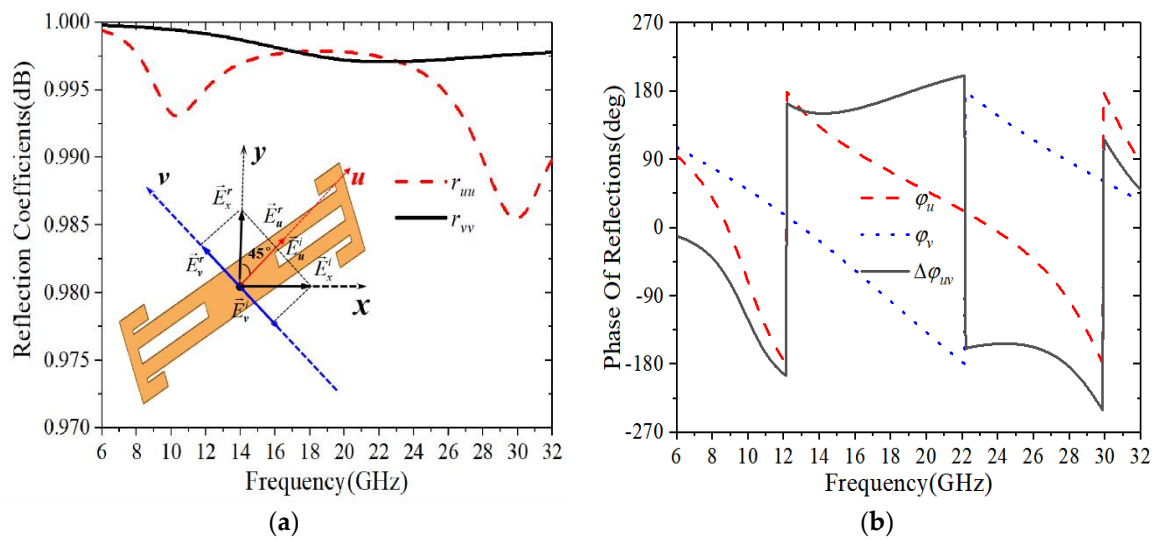


Figure 8. Simulated reflection coefficients of the proposed polarization converter under *u*- and *v*-polarized normal incidences. (a) Amplitude; (b) Phase.

For the lossless case, both of the incident and reflected waves can be regarded as a composite wave composed of *u*- and *v*-polarized components with equal amplitude for *x*-polarized incidence. If the reflection coefficients and phase difference between r_{uu} and r_{vv} satisfy the conditions of [33]:

$$\begin{cases} r_{uu} = r_{vv} = r \\ \Delta\varphi_{uv} = \varphi_{uu} - \varphi_{vv} = \pi \end{cases} \quad (5)$$

a perfect cross-polarization conversion will be formed. If $\Delta\varphi_{uv} \neq 0^\circ$ or $\Delta\varphi_{uv} \neq \pm 180^\circ$, the reflected wave will be elliptically polarized. Specifically, when the phase difference $\Delta\varphi_{uv} = 90^\circ$, the reflected wave will be a circular polarization one, which means that linear to circular polarization conversion is obtained.

Illuminating the structure with polarization along the *u*- and *v*-axes, respectively, the reflection coefficients (r_{uu} and r_{vv}) can be obtained, as plotted in Figure 8a. It is seen that the magnitudes of r_{uu} and r_{vv} are both nearly equal to one (better than 0.98) over the simulation frequency range (6–32 GHz). In addition, there are three minimum values located at 10.36, 22.12 and 29.92 GHz, indicating that three resonance modes are excited by *u*-polarized and *v*-polarized cases, respectively. In fact, the cell of the polarization converter can be equivalent to an LC parallel resonator, wherein the equivalent capacitance *C* are caused by the charge accumulations in the gaps between the adjacent metal patches, and the inductances are created by the metal patches of the polarization converter [36]. Due to the anisotropy of the structure, the values of the equivalent capacitance *C* and inductance *L* are both different at different resonant frequencies, which implies that the *Q* values of these resonant modes are also different [24,36]. However, the phase delay along the *u*-direction and *v*-direction has to be $\pm 180^\circ$ (*n* is an integer) to form a cross polarization converter.

The phase variations and phase difference of r_{uu} and r_{vv} are plotted in Figure 8b. It is seen that there are different phase variations for r_{uu} and r_{vv} at three resonance modes. Evidently, φ_u and φ_v decrease rapidly at the first resonant mode (10.36 GHz), resulting in large phase differences, which make the phase difference $\Delta\varphi_{uv}$ fluctuate around $\pm 180^\circ$ before the appearance of the next resonance mode. Subsequently, the phase difference $\Delta\varphi_{uv}$ can be kept close to $\pm 180^\circ$ for the second resonant mode (22.12 GHz) due to a smaller *Q* value. However, φ_u and φ_v quick asynchronously for the third resonant mode (29.92 GHz), which broke the relative stability of $\Delta\varphi_{uv}$. Therefore, the phase difference $\Delta\varphi_{uv}$ is close to $\pm 180^\circ$ in the frequency range of 10.36–29.92 GHz, showing that the anticipated cross polarization conversion has been realized in this ultra-wide frequency range.

To elaborate further on the physical mechanism behind the polarization conversion, the surface current distributions on the top layer and metallic ground plane are investigated for normal incidence in response to the v - and u -components with various resonant frequencies of 10.36, 22.12 and 29.92 GHz, as shown in Figure 9. It is seen that the current directions on the top and bottom metallic layer are anti-parallel at 10.36 and 22.12 GHz, which implies that a strong magnetic field is generated inside the substrate sandwiched between the two layers. Moreover, a current loop is formed in the intermediate dielectric layer, which is known as magnetic resonance. In contrast, the surface currents of top layer are parallel to those on the background sheet at 29.92 GHz, corresponding to electric resonance. Actually, the ultra-broadband enhancement operation results from the superposition of multiple PCR peaks around resonance frequencies. Therefore, multiple resonances are vital to realize high-efficiency and ultra-broadband cross-polarization conversion.

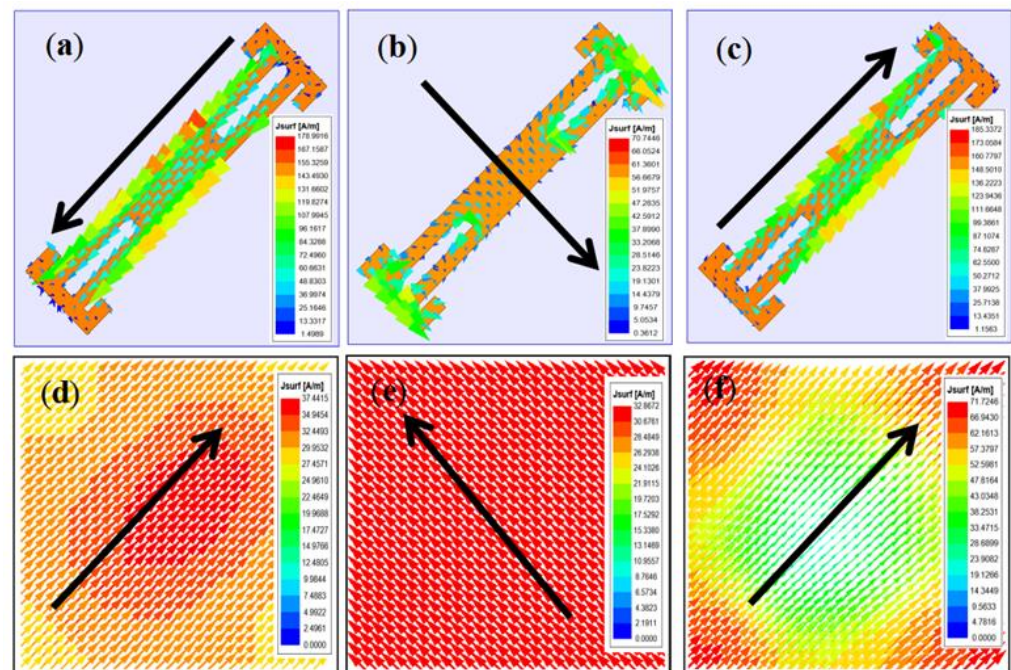


Figure 9. Surface current distributions on top layer and metallic ground plane for normal incidence in response to the v - and u -components with various resonant frequencies of (a,b) 10.36 GHz; (c,d) 22.12 GHz; (e,f) 29.92 GHz.

3.2. Parametric Analysis

3.2.1. Dependence of PCR on Unit Cell Periodicity

A systematic parametric study has been conducted to analyze the sensitivity of some critical dimensions. Since the periodicity p and substrate thickness h of unit cell have a larger dimension versus the length g , s , l_1 , l_2 and l_3 or width w of unit cell, the step is set to 100 μm for p and h , but the length g is less sensitive for dimensional changes, the step is also set to 100 μm . A much smaller step (20 μm) is applied for other parameters. Following this, to investigate the relationship between the sensitivity of each parameter and fabrication accuracy, the PCRs are plotted for various parameters in Figure 10. The periodicity p of unit cell is varied in the range of 5.9–6.1 mm in a step of 0.1 mm, while other parameters are kept constant, as shown in Figure 10a. It is evident that the bandwidth of the working band is decreasing with the increase from 5.9 to 6.1 mm, while the polarization conversion efficiency increases slightly. Considering both operating bandwidth and the performance, the final value of p is chosen as 6 mm.

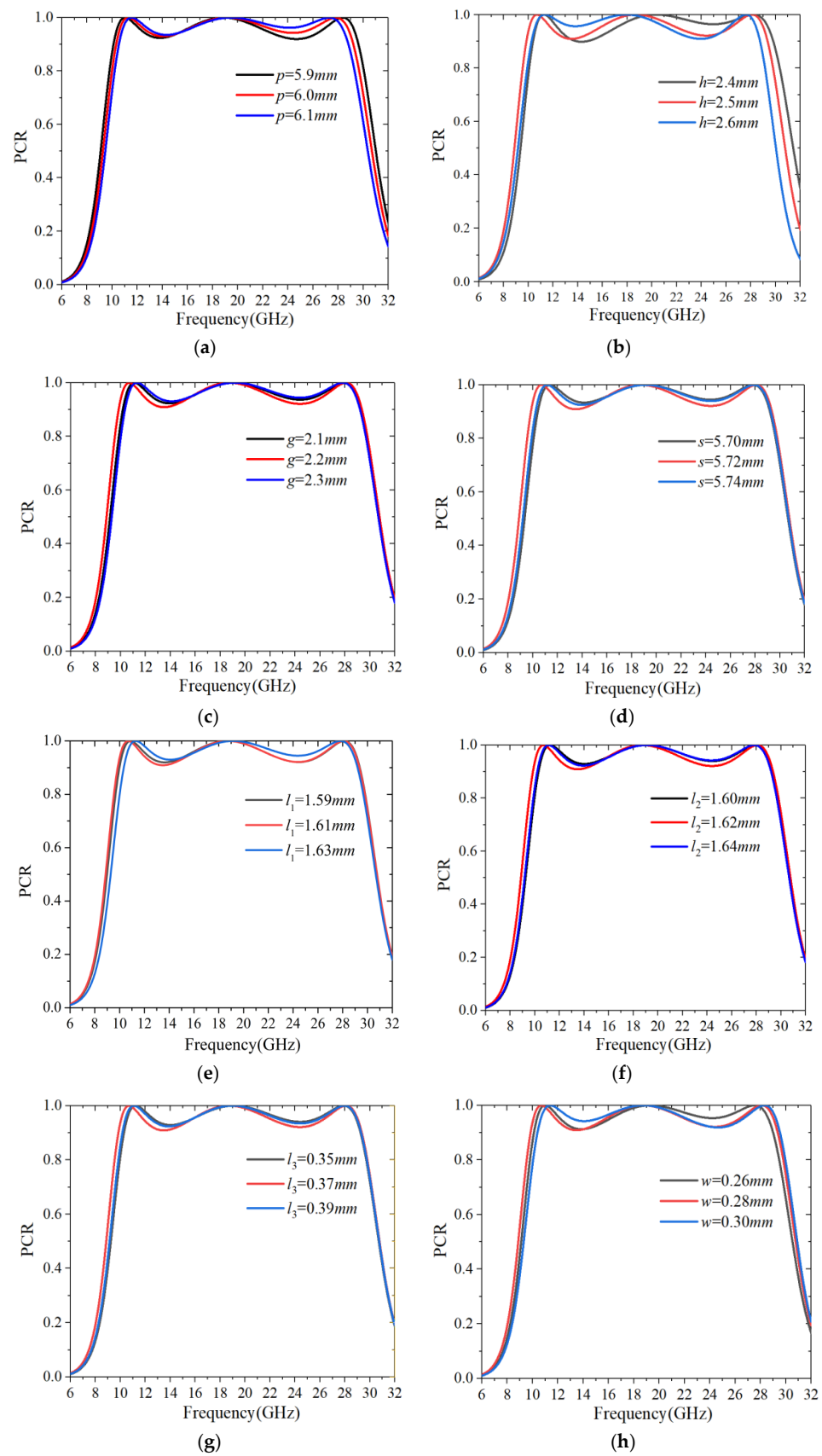


Figure 10. The PCR variation dependence on different parameters of the unit cell. (a) p ; (b) h ; (c) g ; (d) s ; (e) l_1 ; (f) l_2 ; (g) l_3 ; (h) w .

3.2.2. Dependence of PCR on Substrate Thickness

In addition, in order to make the working frequency band meet the requirements of specific applications, the changes of dielectric layer thickness h and other parameters of the unit cell are simulated. Figure 10b shows the PCR of the proposed converter as a function of h in the range of 2.4–2.6 mm without altering the other parameters. Obviously, by increasing h , the operating frequency of the proposed converter is shifted to a lower frequency range. Accordingly, the polarization conversion becomes strong reaching to almost 1 at low frequencies when h increases from 2.4 to 2.6 mm. Contrary to PCR in low frequencies, the PCR reduces to 0.9 with increasing h in high frequencies. Considering the desired broadband performance and commercially available thicknesses of the substrate layer, $h = 2.5$ mm is concluded as the optimized dimension.

3.2.3. Dependence of PCR on Unit Cell Length

After the p and h are determined, Figure 10c–g gives the PCR for various parameters versus the length g , s , l_1 , l_2 and l_3 of unit cell. When g varies from 2.1 to 2.3 mm in 0.1 mm steps, and s , l_1 , l_2 and l_3 increase in 0.02 mm steps, it is evident that in the 14–22 GHz frequency range, the polarization conversion almost remains stable. However, the data curves of the PCR still have a slight shift within the whole frequencies. Furthermore, the response of the PCR for different values of width w of unit cell is also depicted in Figure 10h. When w changes in the range of 0.26–0.3 mm, the polarization conversion efficiency increases slightly at low band, and plays an opposite role at high band. These simulation results imply that 10 μm fabrication accuracy is sufficiently good for this design. The design parameters are determined while considering both operating bandwidth and performance. Based on the above analysis, we can obtain the optimized structure shown in Figure 1.

4. Experimental Results

To verify the design, a prototype is fabricated using the standard print circuit board (PCB) technique. It consists of 41×41 unit cells over an area of $246 \text{ mm} \times 246 \text{ mm}$. The fabricated sample is examined by an industrial microscope, as shown in Figure 11. It can be observed that the fabrication accuracy is well within 10 μm , which is sufficient to obtain the stability of bandwidth and angular incidence.

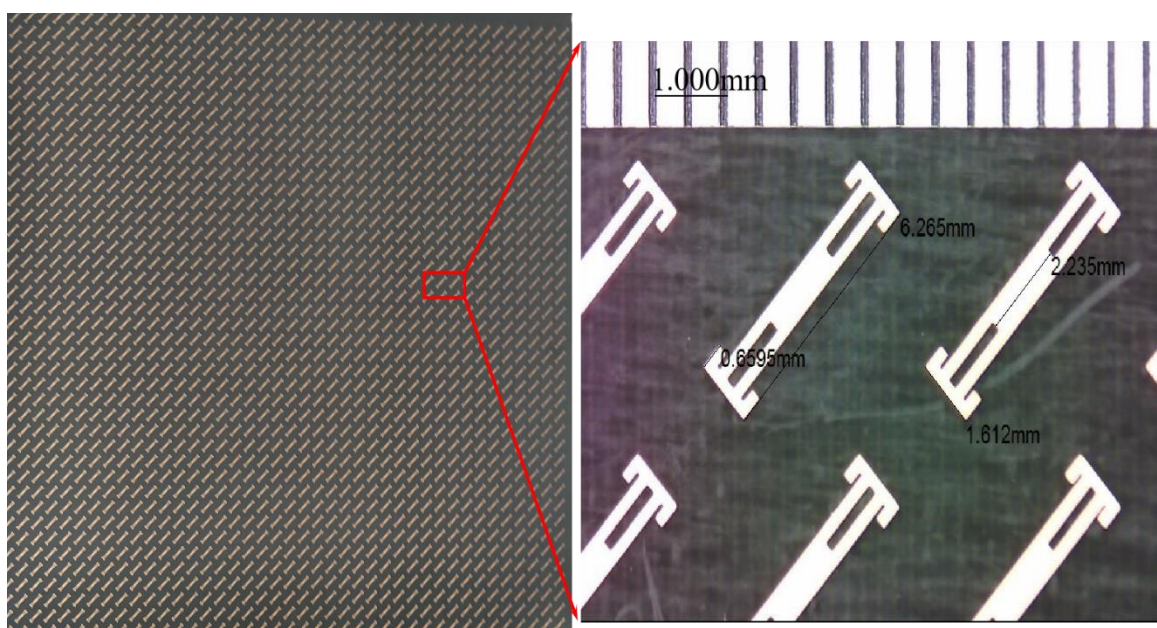


Figure 11. The fabricated sample and its unit cells under an industrial microscope.

The measurement setup is shown in Figure 12. Two horn antennas are connected to a vector network analyzer (Ceyear AV3672D). Radar absorbing materials (RAM) are mounted around the structure to avoid diffraction and spillover from the edge. The horn antennas are placed at the same height to ensure that the EM wave can be illuminated to the center of the structure. For the reflection coefficients measurement, the separation angle between two antennas is set at 5° , which corresponds to the normal incidence measurement in the experiment. By rotating the receiving horn antenna, the test setup is capable of dealing with both horizontal and vertical polarization, so the r_{xx} and r_{yx} can be measured. Moreover, in order to obtain the background, a sheet metal of the same size as the sample is measured to calibrate the system.

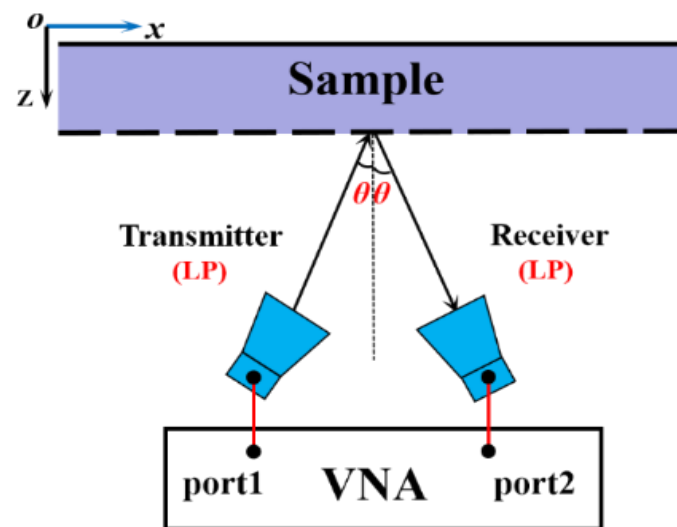


Figure 12. Structure diagram of the measurement setup.

Due to the limitation of our measurement components, the measurement on reflection coefficients is conducted from 15 GHz to 30 GHz. The measured co-polarized and cross-polarized reflection coefficients and the corresponding calculated PCRs at a different oblique incident angle are plotted in Figure 13. It can be seen from Figure 13 that the experimental results are in good agreement with the simulated ones. It has to be mentioned that normal incidence is not measured because of the blockage between the transmitting and receiving horns. Instead, the incident angle of 5° is measured trying to mimic normal incidence. Obviously, at near-normal incidence (oblique angle of 5°), r_{xx} is smaller than -10 dB and r_{yx} is higher than -3 dB in the frequency range of 15–27.42 GHz. Therefore, the calculated PCR is higher than 90%. These results solidly confirm that the illuminated x -polarized wave has been efficiently converted to y -polarized wave after reflection from the converter. Although the PCR decreases with the increase in incident angle, it is always larger than 78% in frequency ranges of 15–23.21 GHz even for a 40° incident angle. Such a result indicates that the proposed converter is insensitive for a wide range of incident angles.

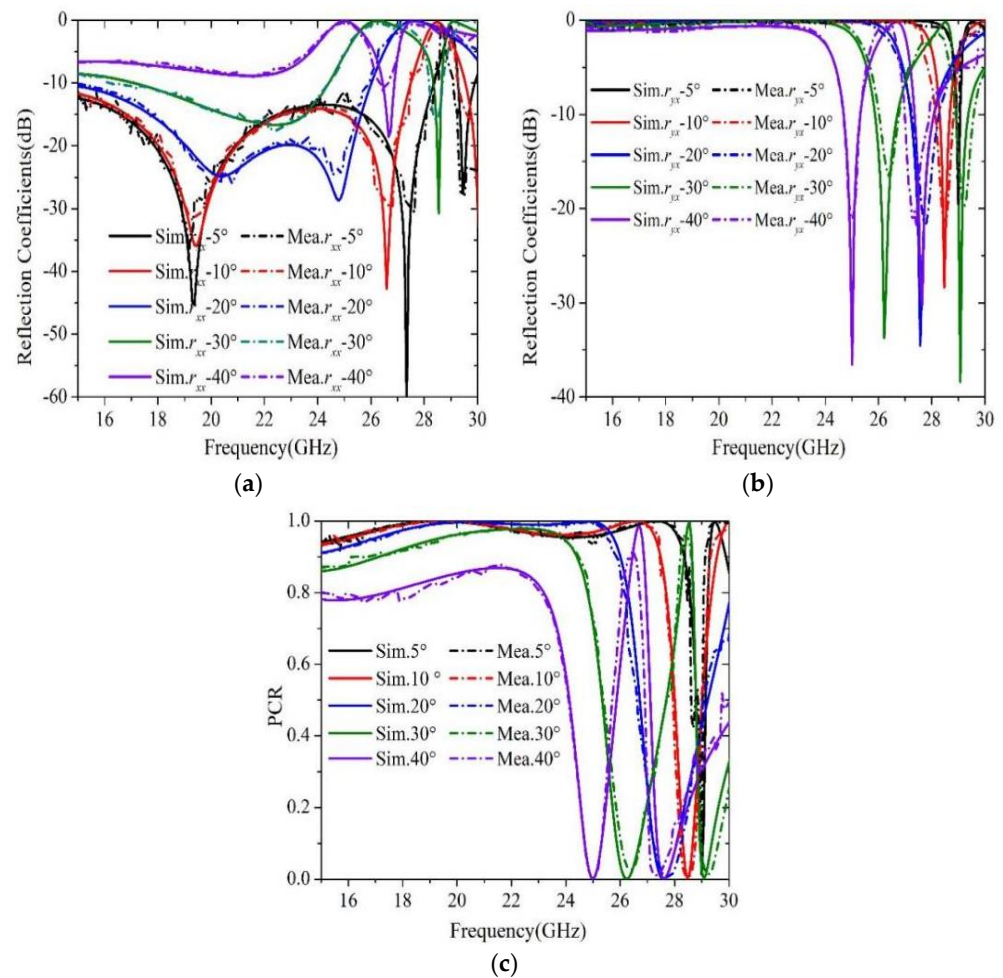


Figure 13. Simulated and measured results for different oblique incident angle. (a) Co-polarized reflection coefficient r_{xx} ; (b) Cross-polarized reflection coefficient r_{yx} ; (c) PCR.

A comparison between the proposed converter with other polarization converters reported recently is presented in Table 1. As can be seen from Table 1, the proposed polarization converter presents a wider bandwidth compared with those reported in Refs. [25–27] and Refs. [31–36]. Although there are a few designs [28–30] that outperform the bandwidth of the one proposed in this work, these structures are developed using via connection or multi-layer dielectric substrates, and only operates efficiently with normal incidence. The presented structure can provide a good angular stability for the oblique incidence angle in Refs. [32–34], but the bandwidth is not wide enough. Both types of broadband design are obtained in Refs. [35,36], but the angular stability is not improved. From the comparison, it can be concluded that good angular stability with satisfactory bandwidth have been realized using the design proposed in this work.

As a matter of fact, it is always a challenge to create large angle stability with a broad bandwidth. One reason is that broadband polarization conversion requires multi-resonances to ensure enough bandwidth. However, for large angle incidence, higher order resonances cannot be always ensured. Therefore, one way is to minimize the unit cell using a folded pattern. However, this will introduce difficulty to the realization of low order resonance. To overcome this difficulty, one may cut slots to prolong the current path so that low order resonance may be obtained. However, if larger angle stability and wider bandwidth are required, these techniques may not be sufficient. Therefore, more techniques may need further investigation.

Table 1. Performance comparison of polarization converters.

Ref.	Frequency (GHz)	Bandwidth	PCR	Thickness	Metallic Layers	Angle Stability
[25]	4.4–5.3, 9.45–13.6	18.56%, 36.01%	90%	$0.044\lambda_{\max}$	2	0°
[26]	7.74–14.44	60.41%	90%	$0.077\lambda_{\max}$	2	0°
[27]	8.2–23	94.87%	80%	$0.082\lambda_{\max}$	2	0°
[28]	6.7–23.4	110.96	90%	$0.073\lambda_{\max}$	2	0°
[29]	16.2–57	111.47%	89%	$0.082\lambda_{\max}$	2	0°
[30]	7.8–34.7	126.56%	90%	$0.104\lambda_{\max}$	3	0°
[31]	10.2–20.5	67%	90%	$0.068\lambda_{\max}$	2	30°
[32]	11.5–21.8	61.86%	90%	$0.076\lambda_{\max}$	2	40°
[33]	17.97–40.23	76.49%	90%	$0.071\lambda_{\max}$	2	40°
[34]	6.36–6.59, 10.54–13.56	3.55%, 25.06%	90%	$0.05\lambda_{\max}$	2	45°
[35]	17–42	84.7%	90%	$0.085\lambda_{\max}$	2	20°
[36]	4.6–12.27	90.93%	90%	$0.076\lambda_{\max}$	2	25°
This work	9.83–29.37	99.69%	90%	$0.082\lambda_{\max}$	2	40°

5. Conclusions

An ultra-broadband reflective polarization converter based on anisotropic metasurface is proposed. The structure converts the linearly polarized incident wave into its orthogonal counterpart over a wide frequency range of 9.83–29.37 GHz. It has been verified that the PCR of the proposed converter is above 90% within the operating band and nearly reaches 100% at three resonant frequencies of 10.68, 18.74 and 28.10 GHz. With surface current distribution analysis, the ultra-broadband polarization conversion is created due to the multiple resonances between top and bottom layers. Moreover, for a wide-angle incidence, this efficiency can be maintained higher than 80%, even though the incident angle reaches 40°. A fabricated prototype is measured, and confirms that the experimental results are in good agreement with the simulation. Compared with other designs in the literature, the proposed polarization converter has a good performance of high efficiency, ultra-broadband and angular stability.

Author Contributions: Conceptualization, X.L.; methodology, B.Z.; software, R.Z. and X.Y.; validation, C.Z.; data curation, B.Z.; writing—original draft preparation, B.Z.; writing—review and editing, X.L.; funding acquisition, X.L., Y.W. and X.Y. All authors have read and agreed to the published version of the manuscript.

Funding: This work is funded in part by the National Natural Science Foundation of China (61871003, 62101005), the Natural Science Foundation of Anhui province (No. 2108085QF256), and Natural Science Research Project for Universities in Anhui Province (KJ2021A0101, KJ2021A1203).

Institutional Review Board Statement: Not applicable.

Informed Consent Statement: Not applicable.

Data Availability Statement: Not applicable.

Conflicts of Interest: The authors declare no conflict of interest.

References

- Xu, J.; Li, R.; Qin, J.; Wang, S.; Han, T. Ultra-Broadband Wide-Angle Linear Polarization Converter Based on H-Shaped Metasurface. *Opt. Express* **2018**, *26*, 20913. [[CrossRef](#)] [[PubMed](#)]
- Yang, Z.; Kou, N.; Yu, S.; Long, F.; Yuan, L.; Ding, Z.; Zhang, Z. Reconfigurable Multifunction Polarization Converter Integrated with PIN Diode. *IEEE Microw. Wirel. Compon. Lett.* **2021**, *31*, 557–560. [[CrossRef](#)]
- Pouyanfar, N.; Nourinia, J.; Ghobadi, C. Multiband and Multifunctional Polarization Converter Using an Asymmetric Metasurface. *Sci. Rep.* **2021**, *11*, 9306. [[CrossRef](#)] [[PubMed](#)]
- Zeng, Q.; Ren, W.; Zhao, H.; Xue, Z.; Li, W. Dual-Band Transmission-Type Circular Polariser Based on Frequency Selective Surfaces. *IET Microw. Antennas Propag.* **2019**, *13*, 216–222. [[CrossRef](#)]
- Li, S.; Zhang, X. Asymmetric Tri-Band Linear-to-Circular Polarization Converter in Transmission Mode. *Int. J. RF Microw. Comput.-Aided Eng.* **2020**, *30*, e21959. [[CrossRef](#)]

6. Liu, K.; Wang, G.; Cai, T.; Li, T. Dual-Band Transmissive Circular Polarization Generator with High Angular Stability. *Opt. Express* **2020**, *28*, 14995. [[CrossRef](#)] [[PubMed](#)]
7. Liao, K.; Liu, S.; Zheng, X.; Zhang, X.; Shao, X.; Kong, X.; Hao, Z. A Polarization Converter with Single-Band Linear-to-Linear and Dual-Band Linear-to-Circular Based on Single-Layer Reflective Metasurface. *Int. J. RF Microw. Comput.-Aided Eng.* **2022**, *32*, e22955. [[CrossRef](#)]
8. Chen, C.-Y.; Hsu, M.-C.; Hu, C.D.; Lin, Y.C. Natural Negative-Refractive-Index Materials. *Phys. Rev. Lett.* **2021**, *127*, 237401. [[CrossRef](#)]
9. Madl, T. Patchy Proteins Form a Perfect Lens. *Science* **2017**, *357*, 546–547. [[CrossRef](#)] [[PubMed](#)]
10. Zhan, J.; Li, K.; Zhou, Y.; Liu, X.; Ma, Y. Ultrathin Conformal Magnetic Invisible Cloak for Irregular Objects. *ACS Appl. Mater. Interfaces* **2021**, *13*, 17104–17109. [[CrossRef](#)]
11. Lin, J.-H.; Yen, T.-J.; Huang, T.-Y. Design of Annulus-Based Dielectric Metamaterial Cloak with Properties of Illusion Optics. *J. Opt.* **2020**, *22*, 085101. [[CrossRef](#)]
12. Tuan, T.S.; Hoa, N.T.Q. Numerical Study of an Efficient Broadband Metamaterial Absorber in Visible Light Region. *IEEE Photonics J.* **2019**, *11*, 4600810. [[CrossRef](#)]
13. Nguyen, T.Q.H.; Nguyen, T.K.T.; Nguyen, T.Q.M.; Cao, T.N.; Phan, H.L.; Luong, N.M.; Le, D.T.; Bui, X.K.; Truong, C.L.; Vu, D.L. Simple Design of a Wideband and Wide-Angle Reflective Linear Polarization Converter Based on Crescent-Shaped Metamaterial for Ku-Band Applications. *Opt. Commun.* **2021**, *486*, 126773. [[CrossRef](#)]
14. Nguyen, T.K.T.; Nguyen, T.M.; Nguyen, H.Q.; Cao, T.N.; Le, D.T.; Bui, X.K.; Bui, S.T.; Truong, C.L.; Vu, D.L.; Nguyen, T.Q.H. Simple Design of Efficient Broadband Multifunctional Polarization Converter for X-Band Applications. *Sci. Rep.* **2021**, *11*, 2032. [[CrossRef](#)] [[PubMed](#)]
15. Wu, X.; Gao, X.; Tang, L. A High-Performance Transmissive Circular Polarization Converter Based on a Modified Fishnet Metasurface. *Appl. Phys. B* **2021**, *127*, 31. [[CrossRef](#)]
16. Wang, L.; Lv, F.; Xiao, Z.; Ma, X. Theoretical and Experimental Verification of 90° Polarization Converter Based on Chiral Metamaterials. *Plasmonics* **2021**, *16*, 199–204. [[CrossRef](#)]
17. Zhang, W.; Li, J.-Y.; Xie, J. A Broadband Circular Polarizer Based on Cross-Shaped Composite Frequency Selective Surfaces. *IEEE Trans. Antennas Propag.* **2017**, *65*, 5623–5627. [[CrossRef](#)]
18. Couto, M.M.; Silva, M.W.B.; Campos, A.L.P.S. A Novel Ultra-Wideband Reflective Cross-Polarization Converter Based on Anisotropic Metasurface. *J. Electromagn. Waves Appl.* **2021**, *35*, 1652–1662. [[CrossRef](#)]
19. Xu, Z.; Sheng, H.; Wang, Q.; Zhou, L.; Shen, Y. Terahertz Broadband Polarization Converter Based on the Double-Split Ring Resonator Metasurface. *SN Appl. Sci.* **2021**, *3*, 763. [[CrossRef](#)]
20. Cui, Z.; Xiao, Z.; Chen, M.; Lv, F.; Xu, Q. A Transmissive Linear Polarization and Circular Polarization Cross Polarization Converter Based on All-Dielectric Metasurface. *J. Electron. Mater.* **2021**, *50*, 4207–4214. [[CrossRef](#)]
21. Liu, D.; Xiao, Z.; Ma, X.; Wang, Z. Broadband Asymmetric Transmission and Multi-Band 90° Polarization Rotator of Linearly Polarized Wave Based on Multi-Layered Metamaterial. *Opt. Commun.* **2015**, *354*, 272–276. [[CrossRef](#)]
22. Naseri, P.; Matos, S.A.; Costa, J.R.; Fernandes, C.A.; Fonseca, N.J.G. Dual-Band Dual Linear to Circular Polarization Converter in Transmission Mode Application to K/Ka-Band Satellite Communications. *IEEE Trans. Antennas Propag.* **2018**, *66*, 7128–7137. [[CrossRef](#)]
23. Zhao, J.; Cheng, Y.; Huang, T.; Liu, P. A Dual-band Linear-to-circular Polarization Converter with Robustness under Oblique Incidences. *Microw. Opt. Technol. Lett.* **2021**, *63*, 361–366. [[CrossRef](#)]
24. Lin, B.; Lv, L.; Guo, J.; Liu, Z.; Ji, X.; Wu, J. An Ultra-Wideband Reflective Linear-to-Circular Polarization Converter Based on Anisotropic Metasurface. *IEEE Access* **2020**, *8*, 82732–82740. [[CrossRef](#)]
25. Huang, X.; Yang, H.; Zhang, D.; Luo, Y. Ultrathin Dual-Band Metasurface Polarization Converter. *IEEE Trans. Antennas Propag.* **2019**, *67*, 4636–4641. [[CrossRef](#)]
26. Zheng, Q.; Guo, C.; Vandenbosch, G.A.E.; Yuan, P.; Ding, J. Dual-broadband Highly Efficient Reflective Multi-polarisation Converter Based on Multi-order Plasmon Resonant Metasurface. *IET Microw. Antennas Propag.* **2020**, *14*, 967–972. [[CrossRef](#)]
27. Li, F.; Chen, H.; Zhang, L.; Zhou, Y.; Xie, J.; Deng, L.; Harris, V.G. Compact High-Efficiency Broadband Metamaterial Polarizing Reflector at Microwave Frequencies. *IEEE Trans. Microw. Theory Tech.* **2019**, *67*, 606–614. [[CrossRef](#)]
28. Zaker, R.; Sadeghzadeh, A. A Low-Profile Design of Polarization Rotation Reflective Surface for Wideband RCS Reduction. *IEEE Antennas Wirel. Propag. Lett.* **2019**, *18*, 1794–1798. [[CrossRef](#)]
29. Omar, A.A.; Hong, W.; Al-Awamry, A.; Mahmoud, A.-E. A Single-Layer Vialess Wideband Reflective Polarization Rotator Utilizing Perforated Holes. *IEEE Antennas Wirel. Propag. Lett.* **2020**, *19*, 2053–2056. [[CrossRef](#)]
30. Jia, Y.; Liu, Y.; Zhang, W.; Gong, S. Ultra-Wideband and High-Efficiency Polarization Rotator Based on Metasurface. *Appl. Phys. Lett.* **2016**, *109*, 051901. [[CrossRef](#)]
31. Karamirad, M.; Ghobadi, C.; Nourinia, J. Metasurfaces for Wideband and Efficient Polarization Rotation. *IEEE Trans. Antennas Propag.* **2021**, *69*, 1799–1804. [[CrossRef](#)]
32. Liu, Z.; Zhao, B.; Jiao, C.; Zhao, L.; Han, X. Broadband Cross-Polarization Conversion Metasurface Based on Cross-Shaped Resonators. *Appl. Phys. A* **2021**, *127*, 825. [[CrossRef](#)]

33. Shukoor, M.A.; Dey, S.; Koul, S.K.; Poddar, A.K.; Rohde, U.L. Broadband linear-cross and circular-circular Polarizers with Minimal Bandwidth Reduction at Higher Oblique Angles for RCS Applications. *Int. J. RF Microw. Comput.-Aided Eng.* **2021**, *31*, e22693. [[CrossRef](#)]
34. Salman, M.S.; Khan, M.I.; Tahir, F.A.; Rmili, H. Multifunctional Single Layer Metasurface Based on Hexagonal Split Ring Resonator. *IEEE Access* **2020**, *8*, 28054–28063. [[CrossRef](#)]
35. Yang, X.; Qi, T.; Zeng, Y.; Liu, X.; Lu, G.; Cai, Q. Broadband Reflective Polarization Rotator Built on Single Substrate. *Electronics* **2021**, *10*, 916. [[CrossRef](#)]
36. Wu, L.-P.; Fang, Q.-H.; Pan, W.-K.; Li, M.-H.; Dong, J.-F. Realizing of Cross-Polarization Conversion for Linearly Polarized Waves in Multiband by Orthotropic Metasurface. *J. Electromagn. Waves Appl.* **2022**, *36*, 101–114. [[CrossRef](#)]
37. Liu, X.; Wang, H.; Yang, X.; Wang, J. Quad-Band Circular Polarized Antenna for GNSS, 5G and WIFI-6E Applications. *Electronics* **2022**, *11*, 1133. [[CrossRef](#)]
38. Gao, X.; Han, X.; Cao, W.-P.; Li, H.O.; Ma, H.F.; Cui, T.J. Ultrawideband and High-Efficiency Linear Polarization Converter Based on Double V-Shaped Metasurface. *IEEE Trans. Antennas Propagat.* **2015**, *63*, 3522–3530. [[CrossRef](#)]